Proceedings of the 2001 IEEE
International Conference on Robotics & Automation
Seoul, Korea · May 21-26, 2001

Good Vibrations: A Vibration Damping Setpoint Controller for Continuum Robots

Ian A. Gravagne*, Christopher D. Rahn†, and Ian D. Walker*
igravag@ces.clemson.edu, cdr10@psu.edu, ianw@ces.clemson.edu

Abstract

In this paper, we focus on a class of robotic manipulators that utilize continuous backbone structures. Such manipulators, known as "continuum" robots, exhibit behavior similar to tentacles, trunks, and snakes. Specifically, we have previously discussed some of the mechanical and kinematic details of the Clemson "Tentacle Manipulator." This work examines the dynamic characteristics of this manipulator, proposing a vibration damping control strategy for configurations with the worst vibration characteristics. We begin by formulating the dynamics for one section of the Tentacle Manipulator. We then proceed to develop a new vibration control strategy which incorporates a setpoint regulator. We supplement the theoretical developments with experimental results.

1 Introduction

The study of hyper-redundant and continuum manipulators finds motivation from the natural world. Even from a qualitative point of view, manipulators such as tentacles and trunks exhibit special capabilities not shared with low degree-of-freedom (DOF) designs. While it is not yet possible to emulate real tentacles or trunks, artificial continuum designs do possess several key desirable features, including improved obstacle avoidance capabilities and a significant transference of weight and complexity away from the actual manipulator, back to a more suitable location. We have previously termed this arrangement "remote actuation" [3], and it allows a substantial reduction in the overall design complexity (and cost) for continuum manipulators such as the Clemson Tentacle Manipulator (figure 1) and the Rice/Clemson Elephant's Trunk Manipulator [3]-[6]. Continuum robots also possess another key feature, termed **inherent compliance**. In other words, the infinite-dimensional kinematics admit an infinity of possible backbone configurations for any given finite set of applied forces or torques along the backbone. Thus, the robot will comply with environmental obstacles or non-conservative loads without the need for expensive and complicated force feedback mechanisms. In principle, the preceding characteristics make continuum and hyper-redundant manipulators suitable for delicate or dangerous tasks where a traditional robot could not reach, or where single-point failures would paralyze subsequent operation of the robot. Examples of such tasks are toxic waste inspection and removal, and navigation or inspection of highly cluttered environments such as collapsed buildings.

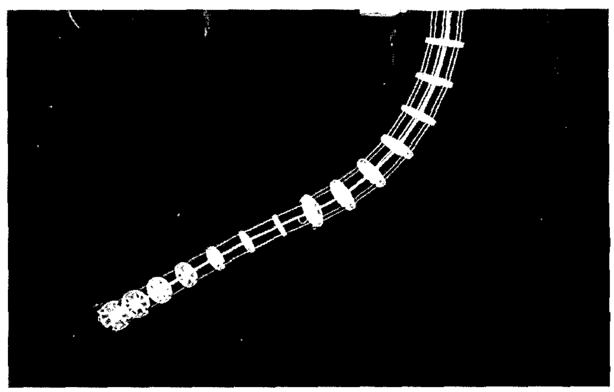

Figure 1: The Clemson Tentacle Manipulator. The manipulator consists of 2 independent sections on a continuous backbone consisting of a thin elastic rod.

In this paper we will focus on a simplified dynamic description of the Tentacle Manipulator, which is a small 2-section (four DOF) experimental prototype. Its backbone consists of a continuous elastic rod, with cable guides periodically spaced along its length. Four cable pairs run through the guide eyelets, two pairs terminating at the midpoint and two at the endpoint. Thus, torques may be applied in orthogonal directions at the midpoint or endpoint of the backbone by exerting tensions on the cables. However, because the backbone is relatively long and slender, sudden movements tend to excite undesirable vibratory motions. The objectives of this paper are to deduce a simplified dynamical description of the backbone by applying a physically reasonable set of constraints and assumptions to the general 3-D dynamics for rods and beams; to apply a simple control law which

*Department of Electrical and Computer Engineering, Clemson University

†Dept. of Mechanical and Nuclear Engineering, Pennsylvania State University.

will permit setpoint regulation of the midpoint and endpoint orientations while improving vibrational damping; and to illustrate the effectiveness of the controller by experimental implementation on the Tentacle Manipulator. In the context of traditional vibration control literature, the Tentacle Manipulator is a 3-dimensional variation on the "clamped-free" beam configuration. However, in contrast to the usual application of boundary shear forces in the clamped-free problem, here only boundary torques are available at the free end. The absence of controllable boundary shear forces distinguishes the current problem, along with our desire to regulate the section orientation to a non-zero setpoint and the multi-dimensional aspect of the dynamics.

Several researchers have addressed topics related to manipulation and locomotion using hyper-redundant and continuum backbones. Among these, the pioneering work of Hirose [1] represented a large step forward in the realization of practical snake-like devices. Chirikjian and Mochiyama, [9]-[12], contributed to the theoretical development of hyper-redundant kinematics, path planning, and shape optimization. Further work in kinematics with a tilt toward practical design considerations appears in [2]-[6]. Another trunk-like prototype can be seen in [8]. Similar to the Elephant's Trunk but significantly larger is the GreyPilgrim "Emma" serpentine manipulator [7]. Robinson and Davies [13] also provide a good overview of work in the area.

2 Rod Dynamics

In order to get the best kinematic properties in a remotely-actuated continuum device (such as maximized workspace and nearly constant curvature deformations), the friction between the cable and the cable guides must be minimized. This frictional component depends on configuration; in other words, it increases significantly as the tension in a cable increases and the backbone bends. Consequently, cable and stand-off friction is minimized near the zero-stress reference configuration, a straight line in this case. Unfortunately, while minimizing cable friction has benefits from a kinematic point of view, lack of friction prevents vibrations in the rod from damping out quickly after a commanded sequence of movements. The naturally antagonistic goals of good kinematic characteristics and fast vibration damping present a challenge to the motion control development, a later topic of this paper.

Pursuant to the observation that vibrations present the biggest challenge near the straight reference configuration, the overall rod dynamics may be substantially simplified. The following development justifies these simplifications. We initially constrain the allowable configurations of a rod of length L to a set of spatial curves $\mathcal{C}$ with the following properties

$$\mathcal{C} = \left\{ \begin{array}{c} \{\underline{p}(s), Q(s)\} : [0, L] \to \Re^3 \times SO(3) \\ \text{with } \|\underline{p}'(s)\| = 1 \end{array} \right\} \tag{1}$$

with $h'(s) \triangleq \frac{dh}{ds}$. This set contains all the duples $\{\underline{p}(s), Q(s)\}$ where $\underline{p}(s) = \left[\begin{array}{ccc} x(s) & y(s) & z(s) \end{array} \right]^T$ is the position of the rod at point s and $Q(s)$ its corresponding orientation tensor. The constraint on the tangent magnitude $\|\underline{p}'(s)\| = 1$ implies non-extensibility of the rod, so that the independent parameter $s \in [0, L]$ represents arc length (look ahead to figure 4). Additionally, we append the following conditions on the allowable configurations:

1. With the triad of inertial elementary basis vectors $\{\underline{e}_1, \underline{e}_2, \underline{e}_3\}$ and the product $Q\underline{e}_i \triangleq \underline{q}_i(s)$, we assume

$$\underline{p}'(s) \cdot \underline{q}_1(s) = 1 \tag{2}$$

2. Where the energy in the rod takes the form $E = \int_0^L f(s)ds + \sum_j g(s_j)$ for $0 \leq s_j \leq L$, we assume

$$E < \infty \Rightarrow f(s) \in \mathcal{L}^\infty \tag{3}$$

Note $f(s) \geq 0$ represents deformation energy distributed throughout the rod, and $g(s_j) > 0$ represents lumped-parameter energy stored in point masses and springs.

Because, by the definition of Q we know that $\left\|\underline{q}_i(s)\right\| = 1$, the first condition combined with (1) implies that

$$\underline{p}'(s) = \left[\begin{array}{ccc} x'(s) & y'(s) & z'(s) \end{array} \right]^T = \underline{q}_1(s) \tag{4}$$

so that the curve tangent is aligned with (and in fact, equal to) the first of the triad of orientation column vectors in Q. We will see the significance of this assumption shortly.

For the second condition, we assume that any "dirac delta" distributions in $f(s)$ are disallowed; intuitively this implies that the rod cannot experience single-point changes in distributed coordinates such as curvatures or positions. Condition 2 does not arise from strictly mathematical arguments; it simply states a physically reasonable assumption motivated by engineering judgement. We continue the dynamic development with derivations of the potential and kinetic rod energies.

2.1 Potential Energy

Consider an infinitesimal change in position on the beam from point s to $s + ds$. During this transition, the local rotational rate of change of the orientation Q is $[\Omega\times] = Q^TQ'$ [19]. Note $[\Omega\times]$ is a skew-symmetric matrix whose associated axial vector is $\underline{\Omega}$; in other words

$$[\Omega\times] = \begin{bmatrix} 0 & -\Omega_3 & \Omega_2 \\ \Omega_3 & 0 & -\Omega_1 \\ -\Omega_2 & \Omega_1 & 0 \end{bmatrix} \Rightarrow \underline{\Omega} = \begin{bmatrix} \Omega_1 \\ \Omega_2 \\ \Omega_3 \end{bmatrix} \tag{5}$$

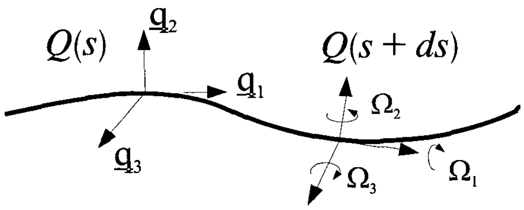

Figure 2: An illustration of the frame $Q(s)$ moving to $Q(s+ds)$ with its associated local angular velocities.

Each element of $\underline{\Omega}$ represents the relative velocity with which each axis in Q is rotating as s moves to $s+ds$. Elements Ω_2 and Ω_3 represent two flexural rotations, and Ω_1 represents torsional rotation, or twist, as can be seen in figure (2). The potential energy in the rod takes the form [15]

$$\begin{aligned} PE &= \frac{1}{2}\int_0^L \left\{\underline{\Omega}^T K_1 \underline{\Omega} + \underline{p}'^T Q K_2 Q^T \underline{p}'\right\} ds \qquad (6) \\ K_1 &= diag\{GJ, EI_1, EI_2\} \\ K_2 &= diag\{EA, GA_2, GA_2\} \end{aligned}$$

For simplicity (and practicality), the robots under consideration have circular cross-sectional backbones, so $EI_1 = EI_2 = EI$ and $GA_1 = GA_2 = GA_s$. In general, we refer to EI as the bending stiffness, GJ as the torsional stiffness, EA as the axial stiffness and GA_s as the shear stiffness. The purely quadratic expression in (6) implicitly assumes small strains; given the aspect ratio (length to thickness) of the rods at hand, small strain is an accurate assumption [20]. (Note that small strains do not necessarily imply small deflections.)

The second component of the potential energy describes energy due to shear deformations of the rod. However, the quantity $\underline{p}'^T Q K_2 Q^T \underline{p}' = EA$ when (2) from condition 1 is taken into account. Thus shear deformations contribute nothing to the overall potential energy, and the axial stiffness contributes only a constant offset which may be neglected without loss of generality. In effect, condition 1 states that the influence of shear may be neglected. Figure (3) offers a pictorial representation of this condition. The robots under consideration in this paper have backbones corresponding to case (B) in figure (3).

At this point we make an important connection with previous kinematic analyses. The potential energy may be written

$$\begin{aligned} \frac{1}{2}\int_0^L \underline{\Omega}^T K_1 \underline{\Omega} ds &= \frac{1}{2}\int_0^L tr\left\{[\Omega\times]^T W_1 [\Omega\times]\right\} ds \\ &= \frac{1}{2}\int_0^L tr\left\{\dot{Q}^T W_2 \dot{Q}\right\} ds \qquad (7) \\ \text{where } W_1 &= diag\left\{EI - \frac{GJ}{2}, \frac{GJ}{2}, \frac{GJ}{2}\right\} \\ \text{and } W_2 &= Q W_1 Q^T \end{aligned}$$

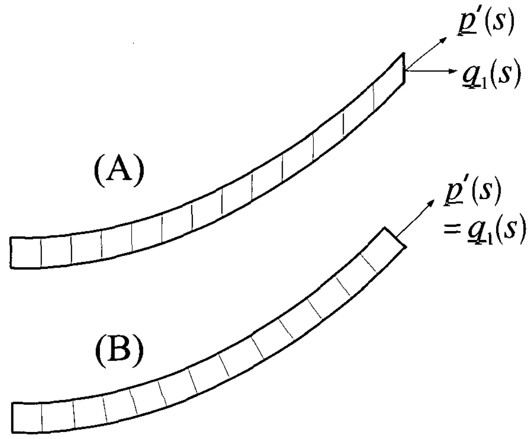

Figure 3: The beam in (A) experiences significant shear deformations because of its resistance to compression and tension along the exterior walls. In (B) shear effects are not present because the concave side has shortened and the convex side as lengthened.

Expression (7) exactly duplicates the optimization measure used by Chirikjian and Gravagne in [3], [4] and [11], [12] for kinematic optimization and analysis, indicating the close connection between those works and the current model. Here, the weighting matrix W_2 is configuration dependent and may not be positive definite; it therefore would not have been an obvious choice apriori. However, this analysis illustrates that continuum kinematics tools and descriptions developed previously still apply to the current physically-motivated model.

2.2 Kinetic Energy

The complete derivation of the kinetic energy is too lengthy to cover here; however, the final result makes intuitive sense. Essentially, we now assume that all quantities composing the potential energy now vary not only with arc length, but also with time. Having the same form as the local spatial rate of rotation seen earlier, the local angular velocity is $[\omega\times] = Q^T\dot{Q}$ with $\dot{Q}$, $\frac{dQ(s,t)}{dt}$. Associating the angular velocity vector $\underline{\omega}$ with its skew-symmetric matrix $[\omega\times]$ in the fashion described previously, we write the kinetic energy as

$$KE = \frac{1}{2}\int_0^L M_\rho \left\|\underline{\dot{p}}(s,t)\right\|^2 + \underline{\omega}^T(s,t) I_\rho(s) \underline{\omega}(s,t) ds \qquad (8)$$

where $I_\rho(s)$ is the rotational inertia density tensor for the reference configuration and M_ρ is the linear mass density of the rod. (Note that neither quantity varies with time.) Both of the expressions for kinetic and potential energy may be seen in similar form with slightly less restrictive conditions in [15].

2.3 Work due to Non-Conservative Forces

In addition to potential and kinetic energy, which arise from conservation principles, energy may be injected or dissipated through the application of forces and torques. On the tentacle robot, there are two sets of cables in orthogonal planes which run down the backbone. Tension in a cable must balance with compressional forces in the beam itself, at every point along its length. Thus, the cable tension represents a distributed conservative input which can perform work. The tensions produce a distributed torque $\underline{\tau}$ about the three axes in Q, proportional to the distance from the backbone to the cable. Since the cables are not directly capable of producing torsional torques, $\underline{\tau} = \begin{bmatrix} 0 & \tau_1 & \tau_2 \end{bmatrix}$ where $\tau_1 = F_1 a(s)$, $\tau_2 = F_2 a(s)$, F_1 and F_2 are the tensions in orthogonal planes, and $a(s)$ is the distance from the cable to the backbone. So the work done to the backbone is

$$W = \int_0^L \underline{\tau}^T \underline{\Omega} ds. \tag{9}$$

In previous work [4], we have discussed that the small spatial variation of $a(s)$ presents some practical design challenges but does not materially detract from the desired kinematic behavior. Thus we consider a as a design constant hereafter.

2.4 Simplifications Due to Small Deflections

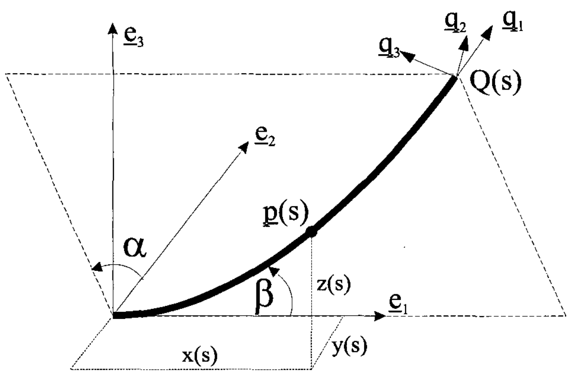

Figure 4: An illustration of how the angles $\alpha(s)$ and $\beta(s)$ contribute to the moving frame $Q(s)$ at any instant in time.

This section concentrates on obtaining a tractable expression for the dynamics of the beam near the straight configuration, which is the area of interest as discussed earlier. First we must make an explicit choice for the orientation tensor $Q(s,t)$. In [4] a we argued for the choice

$$Q(s,t) = Q(\alpha(s,t), \beta(s,t)) \tag{10}$$

$$= \begin{bmatrix} c_\beta & -c_\alpha s_\beta & -s_\alpha s_\beta \\ c_\alpha s_\beta & s_\alpha^2 + c_\alpha^2 c_\beta & -s_\alpha c_\alpha (1-c_\beta) \\ s_\alpha s_\beta & -s_\alpha c_\alpha (1-c_\beta) & c_\alpha^2 + s_\alpha^2 c_\beta \end{bmatrix}$$

with s_α , $\sin(\alpha)$, c_α , $\cos(\alpha)$, etc., as in figure (4). Since the cables cannot produce twists, the angle α remains constant for any particular choice of cable tensions, with [4] showing that $\underline{\tau} = \begin{bmatrix} 0 & F_1 a\cos(\alpha) & F_2 a \sin(\alpha) \end{bmatrix}$.

Next we note that the region of interest for vibration control corresponds to small β (i.e. $\beta < 20°$). Given the restrictions on α and β, the no-shear condition of (2) combined with (10) yields

$$\frac{dx}{ds} \equiv x' = \cos\beta \simeq 1 \Rightarrow ds \simeq dx \tag{11}$$

For all practical purposes we allow $ds = dx$ and, because $x(0,t) = 0\ \forall t$, then x may replace s as the independent spatial variable. A glance back at figure (4) indicates the validity of this statement for "small" deflections. Consequently, we may find the slope of the functions $y(x)$ and $z(x)$ approximated as angles

$$y'(x,t) = \beta(x,t)\cos\alpha \quad \text{and} \quad z'(x,t) = \beta(x,t)\sin\alpha. \tag{12}$$

Evaluating $[\underline{\Omega}\times] = Q(s,t)^T Q(s,t)'$ yields

$$\begin{aligned} \underline{\Omega} &= \begin{bmatrix} 0 & \beta'\cos\alpha & \beta'\sin\alpha \end{bmatrix}^T. \\ &= \begin{bmatrix} 0 & y''(x,t) & z''(x,t) \end{bmatrix}^T. \end{aligned} \tag{13}$$

Referring back to (6) the new expression for the potential energy is

$$PE = \frac{1}{2} EI \int_0^L (y'')^2 + (z'')^2 dx \tag{14}$$

Similarly, we make one further observation that the rotational kinetic energy contributes little compared with the translational kinetic energy, so referring back to (8) reveals

$$KE = \frac{1}{2}\int_0^L M_\rho(\dot{y}^2 + \dot{z}^2) dx. \tag{15}$$

To summarize, these expressions for the system energy require the following simplifications: negligible shear effects, relatively small deflections from the reference configuration, and that the backbone at any instant in time remains planar, or nearly planar.

2.5 Dynamical Equations

Given the analysis this far, we employ the expressions for potential and kinetic energy and non-conservative work in the derivation of the dynamics via Hamilton's Principle. Without demonstration, the results are

$$\begin{aligned} [EIy''(x,t) - \tau_1]'' + M_\rho \ddot{y}(x,t) &= 0 \\ EIy'''(L,t) &= \tau_1'(L,t) \\ EIy''(L,t) &= \tau_1(L,t) \end{aligned} \tag{16}$$

with an identical expression for $z(x,t)$. Similar expressions exist in [14] under the subject of vibration damping using piezo-electric distributed actuators. Here, we have argued that the time-varying distributed torque is spatially constant over $[0, L]$ so the dynamics, with geometric boundary conditions appended, reduce the distributed torque to an equivalent boundary torque,

$$\begin{aligned} EIy''''(x,t) + M_\rho \ddot{y}(x,t) &= 0 && \text{(17a)} \\ EIy'''(L,t) &= 0 && \text{(17b)} \\ EIy''(L,t) &= \tau_1(L,t) && \text{(17c)} \\ y'(0,t) &= 0 && \text{(17d)} \\ y(0,t) &= 0 && \text{(17e)} \end{aligned}$$

with an identical expression for $z(x,t)$.

The decoupled, linear mathematical form of (17), along with energy expressions (15) and (14), could probably have been logically deduced without the need for the extensive preceding derivations. However, in a multi-dimensional problem, there is always the potential for non-linear cross-terms or coupling between the generalized coordinates. Similar complexities here were nullified through the careful application of certain assumptions and observations which may not have been obvious without a derivation from first principles.

3 The Actuator Model

Without loss of generality, we may concentrate on the rod behavior in the x, y plane and assume identical behavior in the x, z plane since the dynamics are decoupled. Next, we note that there is a pulley of radius b to which the cables attach, driven by a motor through a gear ratio of $r > 1$. The angle of the motor is θ_m and the angle of the pulley is θ_p. (The reader may refer ahead to figure 7.) Given that the motor has rotational inertia J and viscous friction B, we may take the simple motor model

$$J\ddot{\theta}_m + B\dot{\theta}_m + \tau_p = \tau_m \tag{18}$$

where $\tau_p = \frac{b}{r}F_1$ is the torque due to the cable tension, and τ_m the torque generated by the motor itself. Note that

$$\theta_m = r\theta_p = \frac{ra}{b}y'(L,t) \tag{19}$$

so that (18) becomes

$$J\frac{ra}{b}\ddot{y}'(L,t) + B\frac{ra}{b}\dot{y}'(L,t) + \frac{b}{r}F_1 = \tau_m \tag{20}$$

Now we choose the feedback control law

$$\begin{aligned} \tau_m &= -k_p\tilde{y}'(L,t) - k_d\dot{y}'(L,t) - k_cF_1 && \text{(21)} \\ \tilde{y}'(L,t) &= y'(L,t) - y'_d \end{aligned}$$

with $k_p, k_d, k_c > 0$ and y'_d the desired boundary angle setpoint. Substituting (21) back into (20) and solving for F_1 produces

$$\tau_1 = aF_1 = -J_{eff}\ddot{y}'(L,t) - K_d\dot{y}'(L,t) - K_p\tilde{y}'(L,t) \tag{22}$$

with

$$\begin{aligned} K_d &= \left[\frac{Br\frac{a^2}{b} + ak_d}{k_c + \frac{b}{r}}\right], \quad K_p = \left[\frac{ak_p}{k_c + \frac{b}{r}}\right], && \text{(23)} \\ J_{eff} &= \left[\frac{Jr\frac{a^2}{b}}{k_c + \frac{b}{r}}\right]. \end{aligned}$$

Because of the relatively high gear ratio r required to bend the rod, (20) suggests that the motor will feel little of the back-driving effect of the rod dynamics transmitted though the cable tension F_1. The coupling factor k_c increases the effective back-driveability of the motor/gear system, providing greater control over the rod boundary. Associating (22) with (17c) results in the new boundary condition

$$EIy''(L,t) + J_{eff}\ddot{y}'(L,t) = -K_d\dot{y}'(L,t) - K_p\tilde{y}'(L,t) \tag{24}$$

4 Controller Stability

Proving the stability of the closed loop system requires two steps: proving the boundedness of the total system energy, and using an invariance principle to illustrate point-wise convergence of the rod to a time independent steady state. We begin by choosing a Lyapunov candidate

$$V = \frac{1}{2}\int_0^L M_\rho\dot{y}^2 + EIy''^2 dx + \frac{1}{2}K_p\tilde{y}'(L,t)^2 + \frac{1}{2}J_{eff}\dot{y}'(L,t)^2 \tag{25}$$

where V consists the distributed rod energy, plus discrete component energies from the effective motor inertia and a virtual spring attached to the free boundary. The power dissipated in this system can then be calculated as

$$\dot{V} = -K_d\dot{y}'(L,t)^2 \leq 0 \tag{26}$$

after accounting for the dynamics in (17) and boundary condition (24). Thus boundedness of the system energy is proven.

Next we wish to explore the possible system solutions if $\dot{V} \equiv 0$. This implies that $\dot{y}'(L,t) \equiv 0$, and to study this case we first note that the dynamics in (17) will admit a separable solution, $y(x,t) = Y(x)W(t)$. So $\dot{y}'(L,t) = Y'(L)\dot{W}(t) \equiv 0$ occurs in two cases.

Case 1: $Y'(L) = 0$. This is simply the zero end-angle situation. Admissible spatial solutions take the form

$$Y(x) = A\cos(kx) + B\sin(kx) + C\cosh(kx) + D\sinh(kx). \tag{27}$$

Manipulation using the boundary conditions indicates $A = -C$ and $B = -D$ and

$$\begin{aligned} A(\sin kL - \sinh kL) + B(-\cos kL - \cosh kL) &= 0 \\ A(-\cos kL - \cosh kL) + B(-\sin kL - \sinh kL) &= 0 \\ A(-\sin kL - \sinh kL) + B(\cos kL - \cosh kL) &= 0 \end{aligned}$$

The coefficients of A and B can be placed in a matrix $M \in \Re^{3\times 2}$ such that

$$M \begin{bmatrix} A \\ B \end{bmatrix} = 0 \tag{28}$$

Direct calculation reveals that $\det(M^T M) > 0 \; \forall k$ which implies that $rank(M) = 2$ and the only solution to (28) is $A = B = 0$, and therefore $C = D = 0$. Thus this case indicates that $y(x,t) = 0$.

Case 2: $\dot{W}(t) = 0$. This implies that $\ddot{y}(x,t) = 0$, so the field equation (17a) suggests $Y''''(x) = 0$. This means $Y'''(x) = c_1$ but $Y'''(L) = 0$ implies $c_1 = 0$. Therefore, $Y''(x) = c_2$ which implies that

$$K_p \tilde{y}'(L,t) = c_2 \tag{29}$$

Consequently, admissible solutions look like

$$W(x) = \frac{1}{2} c_2 x^2 \tag{30}$$

illustrating that $y(x,t)$ is bounded since c_2 is bounded by hypothesis. So it appears that the largest invariant set defined by $\dot{V} \equiv 0$ contains only one point to which the system asymptotically converges: a parabolic rod shape with no time-varying component. Manipulation using the boundary control law reveals that

$$\tilde{y}'(L,t) = \frac{-y_d'}{1 + K_p\left(\frac{L}{EI}\right)} \tag{31}$$

affirming that the steady-state error may be arbitrarily reduced by increasing K_p, an intuitive result.

(In previous work, we have verified that the expected static shape of a rod deformed by pure boundary torques will be semi-circular. The parabolic rod shape above is only accurate insofar as it approximates a circular arc. This approximation is the net effect of the small-deflection assumption.)

From a practical point of view, we also wish to know that the variables comprising the control law (21) will always be bounded. From the Lyapunov argument, we know that $V(t) < \infty$. By inspection, then, we see that $|\dot{y}'(L,t)| < \infty$, $|\tilde{y}'(L,t)| < \infty$ and $\int_0^L EIy''^2 dx < \infty$. Invoking the energy condition from (3), we can see that $y''(x,t) \in \mathcal{L}^\infty$ and so $y''(L,t) < \infty$. Since $aF_1 = y''(L,t)$, then $F_1 < \infty$ and (21) consists of bounded, stable quantities.

We make the final remark that the use of an invariance principle requires a proof of the uniqueness of the solutions for a system of partial differential equations. This is a detailed, time-consuming affair but particulars appear in such references as [17] and [18].

5 Experimental Results

The system was tested using a series of step inputs for the desired angle y_d'. Figure (5) demonstrates the effect

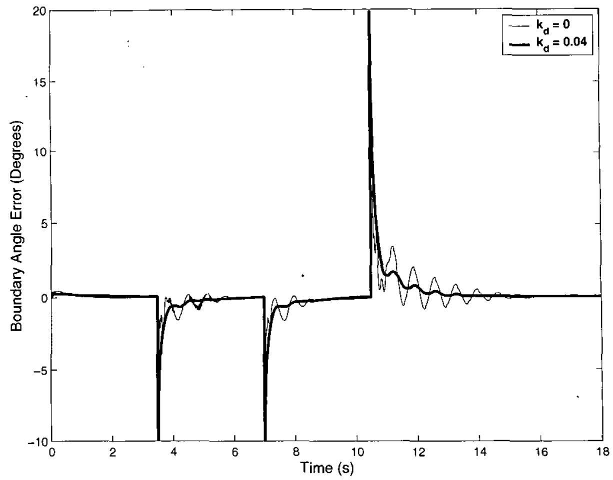

Figure 5: Boundary Angle Error for 3 consecutive step inputs. The first two steps go from 0→10 and 10→20 degrees. The third returns to 0 degrees.

of boundary torque damping on the boundary angle. Experiments support the intuitive conclusion that increasing k_d produces slower step convergence, but increasing k_p too much excites excessive rod dynamics. The compromise in figure (5) requires $k_d = 0.04$, $k_p = 0.38$ and $k_c = 6.0$, resulting in improved vibration damping and a faster settling time. Zooming in on the large step input, figure (6) captures the tension F_1 for both of the previous cases and one more, that of $k_c = 0$. The gear ratio on the tentacle robot is very large, so with no coupling, the desired angle settles within a fraction of a second with disregard for the rod dynamics. Thus, this case results in the worst vibration problem, seen by the dashed line in figure (6).

Throughout the dynamics and control development, we have tacitly assumed that the tension may be a positive or negative quantity. Strictly speaking, of course, tension takes on only positive values. However, for each manipulator section, four cables operate in opposing pairs. Thus the "tensions" we refer to as F_1 and F_2 are actually differential tensions measured by mechanical subtraction. Two load cells convert the differential tensions into electrical signals, one of which is plotted in figure (6). A schematic for this description appears in figure (7).

6 Conclusions

In summary, we began by condensing the general spatial energy expressions for small-strain rods into simpler forms for which the dynamics exhibit greater tractability and usefulness. These simplifications employed a few key assumptions and observations, justifiable for the unique type and design of continuum robots at hand. Subse-

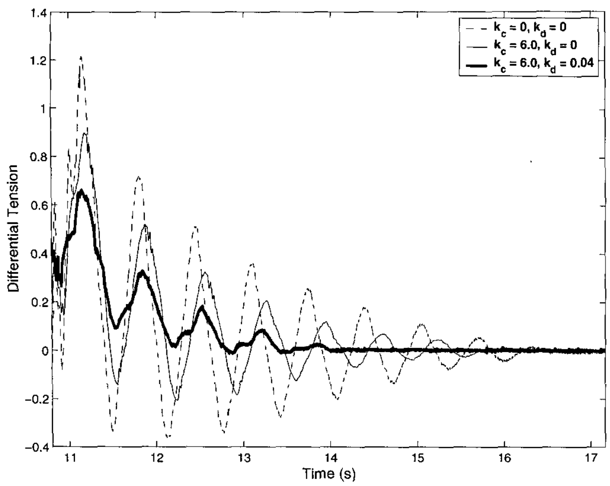

Figure 6: A close up of the tensions for the large step in the previous figure. Also included is the tension for the case with no artificial coupling or damping.

quently, we explored how the actuation system interacts with the dynamics via dynamic boundary conditions, and proposed a proportional-derivative-couple (PDC) controller to help damp out vibrations. The controller was implemented on one section of the Tentacle Manipulator, and experimental results indicate the efficacy of the control law.

Ideally, one would hope in the future to have usable dynamic models for large-scale deflections covering the entire robot workspace. While vibrations certainly present the biggest problem near the origin, we cannot deduce anything about the stability and effectiveness of the proposed controller when the small angle simplifications fail. Distributed forces such as gravity have been left out completely, and little is known about the structural stability of multiple section robots (i.e. buckling and snap-through, not to be confused with dynamic stability). Current work focuses on large deflection dynamic modeling, and the serial connection of multiple sections. Clearly, the modeling efforts are only in their infancy, and the field of continuum and hyper-redundant robots in general presents many unsolved and challenging problems.

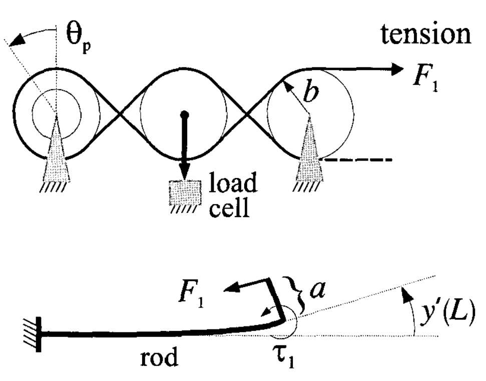

Figure 7: An illustration of how opposing cable tensions are mechanically subtracted for use in the feedback control law.

The authors gratefully acknowledge the support of NASA (grant NAG5-9785), the NSF-EPSCOR program (grant EPS-9630167) and the South Carolina Space Consortium.

References

[1] S. Hirose, **Biologically Inspired Robots**. Oxford University Press, 1993

[2] I.D. Walker and M.W. Hannan, "A Novel Elephant's Trunk Robot", IEEE/ASME Intl. Conf. on Advanced Intelligent Mechatronics, Atlanta, GA, Sept. 1999, pp. 410-415

[3] I. Gravagne and I.D. Walker, "Kinematic Transformations for Remotely-Actuated Planar Continuum Robots," IEEE Int'l Conf. on Robotics and Automation (ICRA), San Francisco, May 2000, pp.

[4] I. Gravagne and I.D. Walker, "On the Kinematics of Remotely-Actuated Continuum Robots," IEEE Int'l. Conf. on Robotics and Automation (ICRA), San Francisco, May 2000.

[5] M. Hannan and I.D. Walker, "Novel Kinematics for Continuum Robots," 7th Int'l Symposium on Advances in Robot Kinematics, Piran, Slovenia, June 2000, pp. 227-238

[6] M. Hannan and I.D. Walker, "Analysis and Initial Experiments for a Novel Elephant's Trunk Robot," Int'l Conf. on Intelligent Robots and System (IROS), Takamatsu, Japan, November 2000, pp. 330-337

[7] GreyPilgrim company, http://www.greypilgrim.com

[8] R. Cieslak and A. Morecki, "Elephant Trunk Type Elastic Manipulator - a Tool for Bulk and Liquid Materials Transportation," Robotica, 1999, Vol. 17 pp. 11-16

[9] H. Mochiyama and H. Kobayashi, "The Shape Jacobian of a Manipulator with Hyper Degrees of Freedom," Proceedings 1999 IEEE Int'l Conf. on Robotics and Automation (ICRA), Detroit MI, May 1999, pp. 2837-2842

[10] H. Mochiyama and H. Kobayashi, "Shape Correspondence between a Spatial Curve and a Manipulator with Hyper Degrees of Freedom," Proceedings 1998 IEEE/RSJ Int'l Conf. on Intelligent Robots and Systems (IROS), Victoria, Canada, October 1998, pp. 161-166

[11] G.S. Chirikjian and J.W. Burdick, "Kinematically Optimal Hyper-Redundant Manipulator Configurations," IEEE Trans. Robotics and Automation, Vol. 11, No. 6, Dec 1995, pp. 794-80

[12] G.S. Chirikjian, "Theory and Applications of Hyper-Redundant Robotic Manipulators," Ph.D. thesis, Dept. of Applied Mechanics, California Institute of Technology, June, 1992

[13] G. Robinson and J.B.C. Davies, "Continuum Robots – A State of the Art," Proc. IEEE Int. Conf. Robotics and Automation, Detroit, MI, May 1999, pp. 2849-2854

[14] S.E. Burke and J.E. Hubbard, "Distributed Actuator Control Design for Flexible Beams," Automatica, Vol. 24 No. 5, pp. 619-627, 1988

[15] J.C. Simo, N. Tarnow and M. Doblare, "Non-Linear Dynamics of Three-Dimensional Rods: Exact Energy and Momentum Conserving Algorithms," Int'l Journal for Numerical Methods in Engineering, V. 38, pp. 1431-1473, 1995

[16] J.C. Simo, L. Vu-Quoc, "On the Dynamics of Flexible Beams under Large Overall Motions – The Plane Case," Journal of Applied Mechanics, Vol. 53, pp.849-863, December 1986

[17] C.D. Rahn, F. Zhang, S. Joshi, and D. Dawson, "Asymptotically Stabilizing Angle Feedback for a Flexible Cable Gantry Crane," ASME Journal of Dynamic Systems, Measurement, and Control, Vol. 121, No. 3, pp. 563-656, September 1999.

[18] C.D. Rahn, **Mechatronic Control of Distributed Vibration and Noise**, Expected Publication Jan. 2001.

[19] M.W. Spong and M. Vidyasagar, **Robot Dynamics and Control**, John Wiley & Sons, 1989

[20] E.H. Love, **A Treatise on the Mathematical Theory of Elasticity**, Dover Publications, NY, 1944